IEEE Access
Multidisciplinary | Rapid Review | Open Access Journal

Received September 6, 2021, accepted September 12, 2021, date of publication September 14, 2021,
date of current version September 21, 2021.

Digital Object Identifier 10.1109/ACCESS.2021.3112902

A Modular Active Balancing Circuit for Redox Flow Battery Applied in Energy Storage System

WEIDE GUAN[1] AND XIAOQING HUANG[2]
[1]School of Electrical and Information Engineering, Changsha University of Science and Technology, Changsha 410004, China
[2]College of Electrical and Information Engineering, Hunan University, Changsha 410082, China

Corresponding author: Weide Guan (guanweide@csust.edu.cn)

This work was supported by the State Key Program of the National Natural Science of China under Grant 51737004.

ABSTRACT To improve the operation performance and energy conversion efficiency of the redox flow battery (RFB), a modular active balancing circuit for redox flow battery applied in the energy storage system is proposed in this paper. Detailed topology description, parameter design, characteristic analysis, operation principle and control strategy of the proposed circuit are presented and discussed in the paper. Different from the conventional battery balancing circuit, the key point of the proposed balancing circuit is that it integrates the circulating pump driving circuit and the state-of-charge (SOC) equalization circuit of the redox flow battery. It uses the energy consumption of the pump driving to balance the SOCs of different battery stacks, which provides a new SOC balancing mechanism for RFB. Based on the proposed circuit, an active balancing control strategy using the time-sharing energy transmission method is proposed, in which the sub-modules of the circuit are alternatively configured in charge-state and discharge-state for absorbing energy or releasing energy to achieve the SOC balancing control for RFB. Compared with the conventional balancing solution or circuit, the proposed modular active balancing circuit simplifies the complexity of the battery management system for RFB, which has the advantages of high efficiency, high reliability, and good scalability. Simulations on Matlab/Simulink and experiments on a downscaled prototype were carried out to verify the feasibility and effectiveness of the proposed circuit and control strategy.

INDEX TERMS Redox flow battery (RFB), active balancing circuit, battery management system (BMS), state-of-charge (SOC) balance, capacitive energy transfer.

I. INTRODUCTION

Renewable energy (RE) sources, such as wind energy and solar energy, have been increasingly used to face concerns over the carbon emission of fossil fuels [1]–[3]. However, the fluctuation and intermittence of renewable energy make it difficult to guarantee a larger proportion to the power grid.

Energy storage system (ESS) has been considered to be the best solution to integrate these renewable energies into future grids [4]–[6]. ESS can provide power quality and energy management services for the grid [7], [8]. Power quality service refers to short time-scale charge and discharge, and energy management service refers to long time-scale charge and discharge.

In actual industrial production, there are many forms of ESS, such as battery energy storage, compressed air energy storage, pumping hydro, mechanical flywheel energy storage, super-capacitors, etc. Compare with other forms of ESS, the battery energy storage system (BESS) has fast and accurate power response-ability, and is becoming the focus on energy storage technology [9], [10]. BESS has a variety of promising battery types, such as lithium-ion (Li-ion) battery, lead-acid battery, sodium-sulphur battery, nickel-hydrogen battery, redox flow battery (RFB), etc.

Compared with other solid-state batteries, RFB has some specific advantages, such as long cycle life, low environmental impact, tolerance of fluctuating power, bearing discharge/charge at high rate, independent rating of power and energy, no self-discharge, etc [11]–[13]. In particular, compared with lithium batteries that often have fire and explosion accidents, RFB has no risk of fire hazards.

Figure 1 shows the basic structure of an RFB. An RFB usually contains one electric stack, two electrolyte tanks, two circulating pumps and some other accessories. The electric stack is composed of multiple electrochemical cells, and each electrochemical cell is composed of two half-cells.

The associate editor coordinating the review of this manuscript and approving it for publication was Shihong Ding.

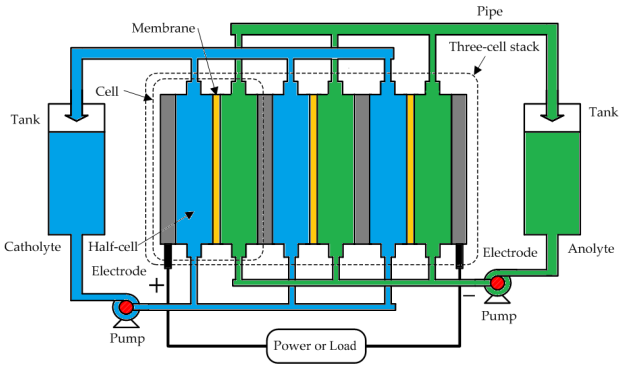

FIGURE 1. Block diagram of redox flow battery (RFB).

Each half-cell is connected to the electrolyte tank that contains metal ions through the pipeline. Positive and negative electrolytes are stored in the two electrolyte tanks. And they are pumped to the ion exchange membrane to generate an electromotive force on the two electrodes due to oxidation and reduction reactions. Once the liquid electrolyte is pumped through the battery, the conversion between electrical and chemical energy will immediately occur at the electrodes. In addition, the electrolytes in the two tanks may be the same or different, depending on different technical methods.

Due to the low output voltage of one single electrochemical cell, which is generally less than 2V, the electric stack of RFB is usually composed of multiple electrochemical cells, electrically connected in series to increase the output voltage [14]. Different from the lead-acid or lithium batteries, there are no issues of cell-balancing among different cells in one stack. Thus, in theory, the more cells in series, the greater the output voltage of the stack. However, as the number of cells in series increases, it will cause problems in the stack, such as shunt current, which will impair the performance and efficiency of the battery. Therefore, the number of cells in one stack is limited [15]–[17]. In addition, too many cells in series will also increase the difficulty of pipeline design.

To increase the power and voltage levels of the RFB energy storage system to meet the industrial demands for the grid, multiple stacks must be connected in series [18]. However, the open-circuit voltage, internal resistance, state-of-charge (SOC) and other parameters of different stacks in the energy storage system will have certain differences due to errors in materials and manufacturing. The worst-performing stack determines the performance of the entire battery. These will decrease the efficiency and performance of the battery during the charging and discharging progress. Eventually, the entire battery will degrade, and the operational lifetime of the battery will decrease because of over-charge or over-discharge.

In order to solve these problems, some publications have studied how to optimize the structural design of the battery to improve the operation performance of RFB. In [19], specific methods for adjusting the composition of electrolytes were proposed to maintain the stability of electrolytes, and obtain the predetermined open-circuit voltage, thereby mitigating the capacity decaying effects of RFB and improving the battery performance. In [20], by adding a balancing cell to the RFB, the imbalance of the battery can be corrected, including both the state-of-charge and proton content of the electrolyte. Ref [21] proposed a balance arrangement and the methods of manufacture for RFB. The proposed solution includes two balancing half-cells and one balanced electrolyte, in which the electrodes of each half-cell keep in contact with its respective balanced electrolyte to balance the SOC of RFB.

Inspired by the balance control methods of lithium batteries and lead-acid batteries, some researchers have begun to study battery balancing methods through external circuits. In general, there are two types of battery balancing circuits, passive balancing circuit and active balancing circuit [22]–[24]. The structure of the passive balancing circuit is simple, but energy loss is a challenge. The active balancing circuit has no energy loss problem, but the circuit structure and its operation are very complicated [25], [26].

T. Zheng *et al.* proposed a SOC balancing control scheme for redox flow battery, in which the super-capacitor was used as an energy carrier to balance the SOC of four RFB batteries [27]. Li *et al.* presented an energy transfer circuit based on the fit capacitance method to realize the SOC balancing of VRB batteries [28]. These two battery balancing methods have been widely used in the SOC balancing control for lithium and lead-acid batteries in the past. Furthermore, patent [29] proposed an expensive solution to balance the SOCs between different stacks, in which separate stacks were connected to individual power converters. Each converter can be modulated individually to adjust the power absorbed or released, and thereby the SOCs can be balanced. Patent [30] proposed an improved method to balance the SOCs among individual stacks for redox flow batteries. By comparing the SOCs of different electrolytes, the method can balance the SOCs of the battery by controlling the number of cells connected in the stack. The number of cells connected in the stack was controlled by switching cells in or out of the stack, in which the switches can be transistor switches or physical switches. However, these above methods are closer to the traditional battery balancing methods of lithium batteries, which have lots of switches, complicated circuits and control strategies.

In summary, the conventional SOC balancing methods for RFB can be roughly divided into three categories, namely, battery structure optimization, passive balancing circuit and active balancing circuit. The comparison of various SOC balancing methods for RFB is shown in Table 1.

The advantage of the battery structure optimization method is that it does not require a separate balancing circuit, but its disadvantage is that the structural optimization is difficult when the number of cells is large, the balancing speed is slow, and the control accuracy is not high enough. Although the method of passive balancing circuit is simple and low in cost, its energy efficiency is too low and it is not suitable for large-capacity energy storage applications. The method of active balancing circuit has high efficiency, but its

TABLE 1. Comparison of different balancing methods.

Methods	Advantages	Disadvantages
Battery structure optimization [19]-[21]	No need of balancing circuit	Difficult to optimize, balancing speed is slow, not accurate
Passive balancing circuit	Easy, cheap	Low efficiency
Active balancing circuit [27]-[30]	High efficiency	High expense and complexity in control

control becomes too complicated as the number of batteries increases.

In order to reduce the complexity of the SOC balancing control system, this paper proposes a modular active balancing circuit for RFB applied in the energy storage system.

As mentioned earlier, RFB has a unique feature, it requires a pump to drive the electrolyte to work, and the pump requires energy. In the conventional RFB control system, the driving circuit of the pump is powered by an external power source, which is independent of the battery balancing circuit.

Different from the conventional battery balancing circuit, the key point of the proposed balancing circuit is that it integrates the circulating pump driving circuit and the SOC equalization circuit together, and uses the energy consumption of the pump to achieve the SOC balancing control between different battery stacks, which can reduce the complexity of the battery control system without wasting energy. In a word, the proposed balancing circuit is different from the balancing circuit of the redox flow battery in the existing literature due to the different operating principle. The balancing circuit proposed in this paper has the advantages of high efficiency, high reliability, and good scalability. Up to now, very few literatures have proposed the same or similar solutions to redox flow battery.

The rest of this paper is organized as follows. In Section II, the circuit topology and operation principle are introduced and described. Section III gives the design and analysis of the proposed circuit. Simulation results based on MATLAB/Simulink software and experimental results based on a downscaled prototype are provided and explained in Section IV and Section V, respectively. Finally, Section VI summarizes this paper.

II. CONFIGURATION AND OPERATION

A. CIRCUIT CONFIGURATION

Figure 2 is the schematic diagram of an RFB modular active balancing circuit applied to an energy storage system. It includes an RFB energy storage system and a modular active balancing circuit. The RFB is connected to the grid through a power conversion system (PCS). The modular active balancing circuit realizes the balancing of SOC for RFB. The active balancing circuit consists of N sub-modules (SMs) and one DC-DC converter. All SMs are cascaded into

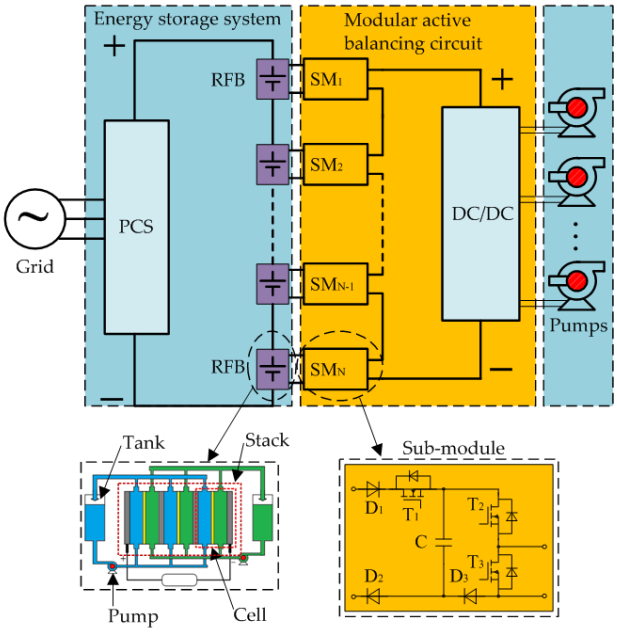

FIGURE 2. The schematic diagram of the modular active balancing circuit for redox flow battery applied in energy storage system.

a string to provide DC power to the DC-DC converter, and each SM contains three diodes, three MOSFETs, and one capacitor. The DC-DC converter drives the circulating pumps of the redox flow battery.

For the circuit, modular sub-modules are connected in parallel with each stack of RFB, and all sub-modules are connected in series to supply power to the circulating pump. When the RFB is discharged, if the SOC of one or several stacks is higher than other stacks, increase the discharge time of these stacks, and these stacks will discharge more. When the RFB is charged, if the SOC of one or several stacks is higher than other stacks, reducing the charging time of these stacks will decrease the charging capacity of these stacks. In this way, the energy consumption of the pump is used to balance the SOC of stacks without wasting energy.

Figure 3 shows two possible working states of the SM. The MOSFETs switch the working states of the SM. The capacitor is used to absorb energy from the battery and release energy to the DC-DC. The diodes control the direction of the current in the circuit to prevent unnecessary reverse current and ensure the normal operation of the circuit.

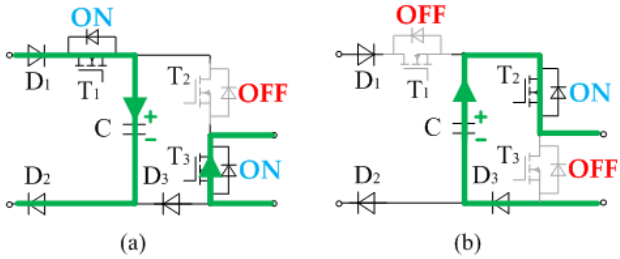

FIGURE 3. Working states of the sub-module: (a) charge state, (b) dis-charge state.

When T_1 and T_3 are turned on, and T_2 is turned off (charge state), the capacitor absorbs energy from the battery; When T_1 and T_3 are turned off, and T_2 is turned on (dis-charge state), the capacitor releases energy to DC-DC converter to drive the circulating pumps. By controlling the duration of ON and OFF, the energy absorbed from the battery stack can be adjusted. Therefore, the SOCs of the battery can be balanced between different stacks.

The balancing circuit proposed in this paper has the advantages of high efficiency, high reliability, and good scalability. First, the proposed circuit uses the energy consumption of the pump to achieve the SOC balancing control. It can reduce the complexity of the battery control system without wasting energy, which improve the energy efficiency of the system. Second, if some of the sub-modules fail, they can be bypassed by the bypass switches, thereby improving the reliability of the system, that is, increasing the redundancy of the system. Third, the modular active balancing circuit for RFB can be easily customized. It can adapt to different voltage and power levels by changing the number of series connections. The hardware configuration is very simple to implement, which is helpful for the upgrade and expansion of the energy storage system. In addition, the proposed balancing circuit does not have high requirements for the consistency of the battery stacks, therefore, RFB stacks with large differences in parameters can be mixed.

B. PRINCIPLE OF OPERATION

As mentioned in the previous section, the sub-module works in two switching states, namely the charge-state and the discharge-state, which are listed in detail in Table 2.

TABLE 2. Working state table of the sub-module.

Switching state	Working state	MOSFET state	Output voltage
$S_k = 0$ [a]	Charge-state	T_1 and T_3 are on, T_2 is off	Zero
$S_k = 1$	Discharge-state	T_1 and T_3 are off, T_2 is on	Capacitor voltage

[a] S_k is the switching state of the ith sub-module ($k = 1,2,\ldots,N$).

As can be seen from Table 2, the output voltage of SM is determined by its working state. For charge-state: the capacitor of SM is charged from the battery, and the output voltage of the SM is zero. For discharge-state: the capacitor supplies the load, and the output voltage of the SM is equal to the capacitor voltage.

The balancing circuit alternatively configures the SMs in charge-state for absorbing energy from the stacks of battery, and then in discharge-state for releasing energy to DC-DC converter to drive the circulating pump.

Figure 4 shows the operation waveforms of the proposed balancing circuit, and the control cycle is T_{cyc}.

During $[0, T_{on}]$, $S_k = 0$, MOSFET T_1 and T_3 are turned on, and T_2 is turned off; The diodes D_1 and D_2 are conducting, and D_3 is reverse biased to block the battery voltage. Thus, the capacitor is connected to the battery stack to absorb

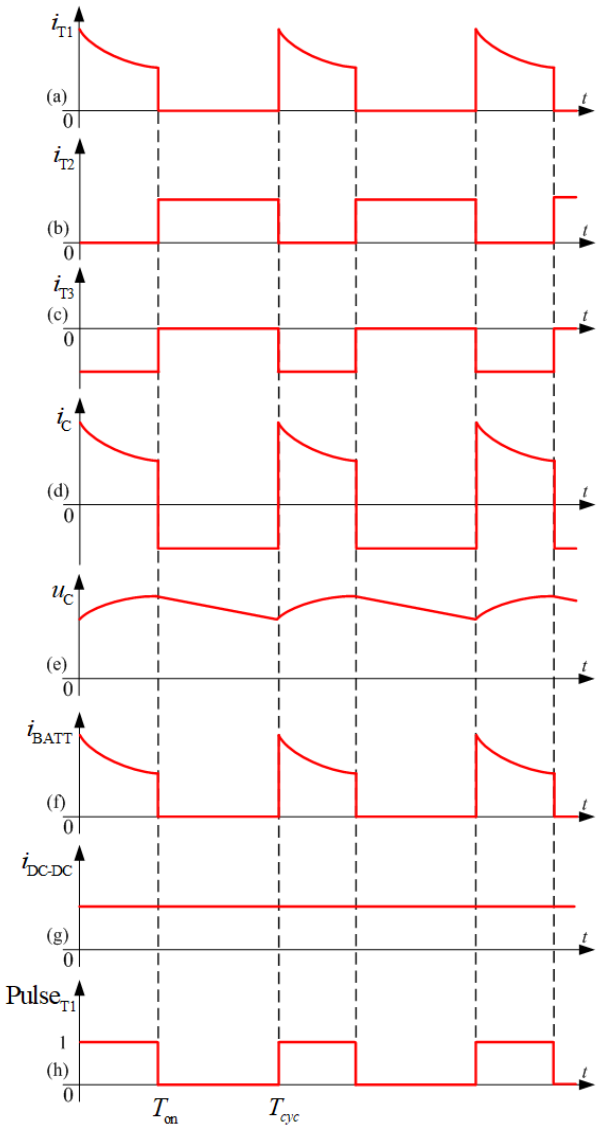

FIGURE 4. Sketched waveforms for the operation of the balancing circuit.

energy from the battery stack, and T_3 provides a freewheeling channel for other SMs. That is, the stack of battery is isolated from the DC-DC converter by the diode D_3. During this period, MOSFET T_1 is turned on and charges the capacitor C. The MOSFET current i_{T1} comes from the battery current i_{BATT}, and is equal to the capacitor current i_C. Therefore, i_{T1} decreases exponentially and capacitor voltage u_C increases exponentially. Meanwhile, the MOSFET current i_{T2} is zero because T_2 is turned off, and the MOSFET current i_{T3} is negative due to freewheeling.

In contrast, during $[T_{on}, T_{cyc}]$, $S_k = 1$, T_1 and T_3 are turned off, and T_2 is turned on; The diode D_3 is conducting, and D_2 is reverse biased to block the battery voltage. Thus, the capacitor releases energy to the DC-DC converter to drive the circulating pump, and the stack of battery is isolated from the DC-DC converter by the diodes. During this period, MOSFET T_2 is turned on and supplies the DC-DC converter.

The MOSFET current i_{T2} comes from the capacitor current i_C, and is equal to the DC-DC current i_{DC-DC}. Therefore, the capacitor voltage u_C decreases with the discharge time. Meanwhile, the MOSFET current i_{T1} and i_{T3} both are zero because T_1 and T_3 are turned off.

It is easy to know that the input current of the sub-module i_{BATT} is intermittent due to the switching action. But the output current i_{DC-DC} is still continuous because it is affected by the freewheeling effect. In addition, the battery and the DC-DC converter are always isolated by diodes. In other words, the battery and the DC-DC converter only exchange energy through the time-sharing access of the capacitor.

III. DESIGN AND ANALYSIS

A. MODEL

Figure 5 shows the equivalent circuit model of the redox flow battery. The equivalent circuit model can characterize the charge and discharge characteristics of the redox flow battery. It has a simple structure, which is convenient for operation and observation of the results, and is conducive to simulation research.

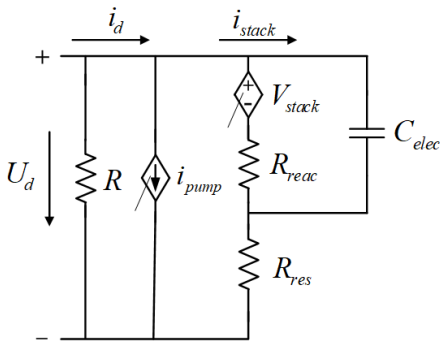

FIGURE 5. Equivalent circuit model of the redox flow battery.

In the equivalent circuit model, U_d is the open-circuit voltage, i_d is the terminal current, i_{pump} is the pump current, V_{stack} is the stack voltage, i_{stack} is the stack current, R_{reac} and R_{res} are the equivalent internal resistance loss, R is the fixed resistance losses, and C_{elec} is the dynamic response capability.

In the model, R_{reac} represents the resistance caused by reaction kinetics, and R_{res} represents the resistance caused by mass migration, membrane, electrode, and bipolar plate. R_{reac} and R_{res} are all RFB equivalent internal resistances. In general, the equivalent internal resistance loss is about $15\%P_{stack}$. And estimate R_{reac} based on $9\%P_{stack}$, and R_{res} based on $6\%P_{stack}$. The calculation formulas are as follows:

$$R_{reac} = \frac{9\%P_{stack}}{i_{stack}^2} \tag{1}$$

$$R_{res} = \frac{6\%P_{stack}}{i_{stack}^2} \tag{2}$$

where P_{stack} is the stack power.

According to the model, the stack current can be expressed:

$$i_{stack} = i_d - i_{pump} \tag{3}$$

i_{pump} represents the pump loss current, which is equivalent to a controlled current source in the model. It can be expressed as:

$$i_{pump} = \frac{ki_{stack}/SOC}{U_d} = 1.011\frac{i_{stack}}{SOC} \tag{4}$$

It can be seen from (4) that i_{pump} varies according to the battery capacity SOC. The larger the SOC, the smaller the i_{pump}.

SOC represents the state-of-charge of the battery. It also represents the ratio of the remaining SOC of the battery to the maximum SOC of the battery. It can be calculated by:

$$SOC_t = SOC_{t-1} + \Delta SOC \tag{5}$$

$$\Delta SOC = \frac{\Delta E}{E_N} \approx \frac{V_{stack}i_{stack}\Delta t}{E_N} \tag{6}$$

where SOC_t represents the SOC at the current moment, SOC_{t-1} represents the SOC at the previous moment, ΔSOC represents the incremental SOC, E_N represents the battery capacity, Δt represents the simulation step size, and V_{stack} represents the RFB stack voltage, which is equivalent to a controlled voltage source in the model.

In order to study the natural characteristics of RFB, in the simulation experiment, the RFB's SOC is estimated through the stack voltage V_{stack}. However, in actual application, it is difficult to detect the RFB's stack voltage V_{stack}. Therefore, the SOC of RFB is generally estimated by detecting the terminal voltage U_d of the RFB.

Figure 6 shows the equivalent circuit of the proposed active balancing circuit for redox flow battery applied in the energy storage system. In the circuit, each sub-module connected to the redox flow battery is equivalent to a controlled voltage source. All sub-modules are connected in series to form a total DC voltage to supply the DC-DC converter.

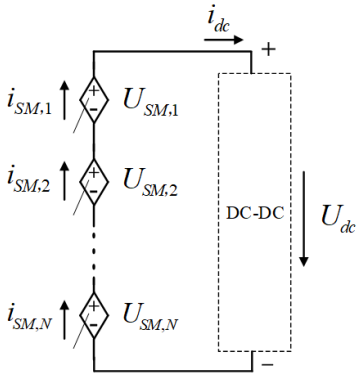

FIGURE 6. Equivalent circuit of the modular active balancing circuit.

From the equivalent circuit, the voltage and current of the DC bus can be expressed as follows:

$$U_{dc} = \sum_{k=1}^{N} U_{SM,k} \tag{7}$$

$$i_{dc} = i_{SM,1} = i_{SM,2} = \cdots = i_{SM,N} \tag{8}$$

where $U_{SM,k}$ and $i_{SM,k}$ are the output voltage and current of the kth sub-module, $k = 1, 2, \ldots, N$.

Based on the operation principle in the previous section, the output voltage of each sub-module can be defined as:

$$U_{SM,k} = S_k u_{C,k} \approx S_k U_{dc}/M \tag{9}$$

where $u_{C,k}$ is the capacitor voltage of the kth sub-module, and M is the instantaneous number of sub-modules in the discharge state.

According to (7) - (9), the instantaneous output power of each sub-module can be expressed as:

$$P_{SM,k} = U_{SM,k} i_{SM,k} = S_k u_{C,k} i_{dc} \tag{10}$$

When the switching frequency is fast enough, the capacitor voltage of each sub-module can be regarded as a constant value. Therefore, the output power of each sub-module depends on the length of time connected in series in the circuit.

Therefore, the SOC of each stack of the redox flow battery can be balanced by adjusting the switching duty cycle of the corresponding sub-module.

B. DESIGN

SM capacitor is designed to buffer the energy fluctuation during charging and discharging. In each control cycle, the energy absorbed from the battery should be equal to the energy released to DC-DC. Therefore, the energy variation of each capacitor can be calculated by integrating its power during the charging period [0, T_{on}], as follows:

$$\Delta E = \int_0^{T_{on}} u_{C,k} i_{C,k} dt = \int_{T_{on}}^{T_{cyc}} \frac{U_{dc}}{M} i_{dc} dt \approx \frac{U_{dc} I_{dc} T_{on}}{M} \tag{11}$$

where I_{dc} is the average input current of the DC-DC converter.

The energy variation of each capacitor is reflected as the voltage fluctuations, namely,

$$\Delta E = \frac{1}{2} C \left(u_{c,\max}^2 - u_{c,\min}^2 \right) = \varepsilon C \left(\frac{U_{dc}}{M} \right)^2 \tag{12}$$

where ε is the capacitor ripple coefficient, $u_{c,\max}$ and $u_{c,\min}$ are the maximum and minimum voltages of the capacitor, respectively.

According to (11) and (12), the calculation formula for the capacitance value of the sub-module capacitor can be obtained as follows:

$$C = \frac{M I_{dc} T_{on}}{\varepsilon U_{dc}} \tag{13}$$

As shown in Figure 2, the whole balancing circuit contains N SMs, and each SM contains 3 MOSFETs and 3 diodes, so there are $3N$ MOSFETS and $3N$ diodes in total.

According to the current waveform in Figure 4, the current stress of the MOSFET and diode is determined by the maximum charging or discharging current of the capacitor. It can be expressed as

$$i_{stress} = MAX \left(i_{C,ch\,a,\max}, i_{C,dis,\max} \right) \tag{14}$$

where $i_{C,cha,max}$ is the maximum charging current of the capacitor, and $i_{C,dis,max}$ is the maximum discharging current of the capacitor.

The maximum charge current of the capacitor can be calculated by:

$$i_{C,ch\,a,\max} = \frac{u_{stack,\max} - u_{C,\min}}{R} \tag{15}$$

where $u_{\text{stack},max}$ is the maximum voltage of the stack of redox flow battery, $u_{C,min}$ is the minimum voltage of the capacitor, and R is the equivalent internal resistance of charging circuit.

The discharge current of the capacitor is determined by the whole discharging circuit, which includes M SMs and the DC-DC converter. Thus, the maximum discharge current of the capacitor is equal to the maximum DC load current, which can be expressed by:

$$i_{C,dis,\max} = i_{dc,\max} \tag{16}$$

where $i_{dc,max}$ is the maximum input current of the DC-DC.

According to the topology and working principle in Figure 2 and 3, the voltage stresses of the MOSFETs and diodes are determined by the maximum voltage difference between the left part and right part of the balancing circuit, which can be expressed as:

$$u_{stress} = (N-1) u_{stack,\max} \tag{17}$$

Therefore, in the actual industrial design, the parameter of MOSFETs and diodes can be calculated based on the above-mentioned maximum voltage and current stress to ensure safety.

C. CONTROL SCHEME

Figure 7 presents the control block diagram of the active balancing circuit. The control scheme can ensure the normal operation of the proposed active balancing circuit.

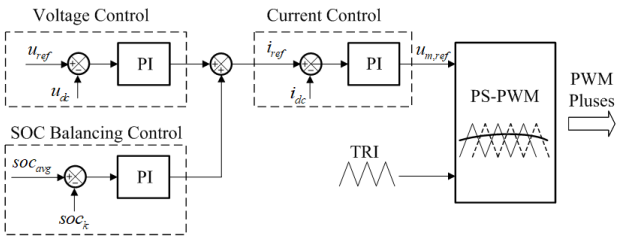

FIGURE 7. Control block diagrams of the active balancing circuit.

There are three controllers for the proposed scheme, voltage controller, current controller, and SOC balancing controller. The voltage controller and current controller transfer energy to the DC-DC while the SOC of stacks of redox flow battery is balanced by the SOC balancing controller.

According to the difference between reference voltage u_{ref} and actual voltage u_{dc} of the circuit, the voltage controller

generates a general inner current reference i_{ref}. Meanwhile, SOC balancing controller adjusts the inner reference current i_{ref} by comparing the average SOC soc_{avg} and actual SOC soc_k of each stack of the redox flow battery. Then all the SMs are controlled by the current controller, getting the modulating voltage references $u_{m,ref}$. The above three controllers can use conventional proportional integral (PI) control method or other nonlinear control algorithms, such as sliding mode control (SMC) [31], [32], adaptive control [33], fuzzy control [34], model predictive control [35], and so on. Finally, these voltage references are modulated by the triangular carriers in the phase-shift pulse width modulation (PS-PWM) block, obtaining the gating signals to drive the MOSFETs.

IV. SIMULATION VERIFICATION

To verify the feasibility of the proposed balancing circuit and its control scheme, a simulation model of the modular active balancing circuit for redox flow battery applied in the energy storage system was investigated on MATLAB software.

According to Figure 2, the simulation model includes an energy storage system and a modular active balancing circuit. RFB is connected to the power grid by PCS. The RFB consists of 8 stacks, and each stack contains 32 cells. The modular active balancing circuit consists of 8 SMs and one DC-DC converter. Detailed parameters of the simulation model are listed in Table 3. It should be noted that in order to see the control effect in a short time, the battery capacity parameter is set very small, which is only 0.05 Ah.

TABLE 3. Parameters of simulation model.

Parameter	Value
Rated DC bus voltage of PCS (V)	384
Number of stacks	8
Rated voltage of the stack (V)	48
Rated capacity of one stack (Ah)	0.05
Number of SMs of balancing circuit	8
Number of cells per stack	32
Rated voltage of one cell (V)	1.5
Rated voltage of DC load (V)	150
Rated current of DC load (A)	30
Sampling period (μs)	200

Figure 8 shows the simulation results of SOC balancing control for redox flow battery when the battery is discharged and charged, respectively. At t = 0s, the initial SOC of each stack is different, and its value varies between 50% and 54%. Then balancing control scheme is enabled. At t = 0.6s, the voltages of all stacks tend to be the same. Figure 8(a) shows the balancing control results of discharging process, and Figure 8(b) shows the results of the charging process.

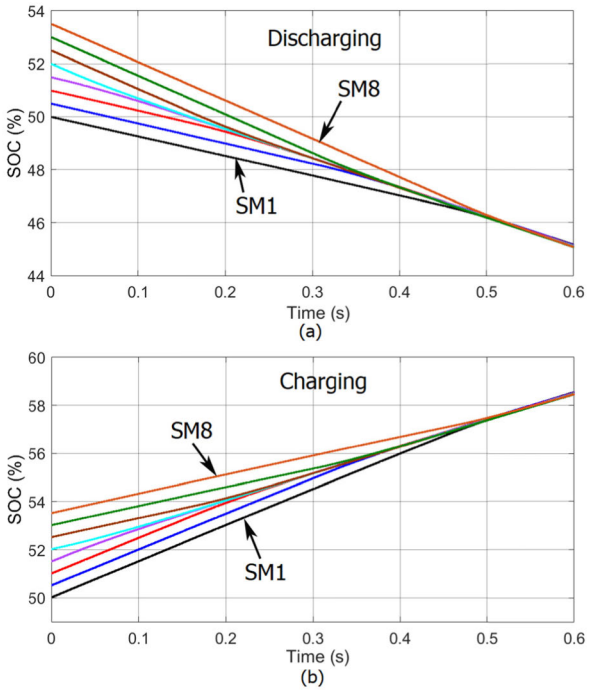

FIGURE 8. Simulation results of the SOC balancing control for the redox flow battery: (a) discharging process, (b) charging process.

Table 4 lists the battery SOC value before and after the balance control. It can be seen that whether it is charged or discharged, the SOCs of stacks have been balanced very well.

TABLE 4. RFB stack SOC value of simulation model.

Serial of stack	Initial SOC (%)	SOC after discharging (%)	SOC after charging (%)
1	50.0	45.3	58.5
2	50.5	45.2	58.5
3	51	45.2	58.4
4	51.5	45.1	58.4
5	52	45.1	58.4
6	52.5	45.0	58.3
7	53	44.9	58.3
8	53.5	44.9	58.2

As mentioned in Section I, the energy absorbed from the RFB stack can be adjusted by controlling the duty cycle of the PWM. Therefore, the SOCs of the battery can be balanced between different stacks.

Figure 9 shows the simulation current waveforms of the SMs before the SOC balancing was completed during the discharging process. At t = 0.025s, the SOC of the battery is not balanced, thus the input currents of the 8 SMs differ greatly. SM5, SM6, SM7 and SM8 with higher SOC are more discharged, and SM1, SM2, SM3 and SM4 with lower SOC are less discharged.

Figure 10 shows the simulation current waveforms of the SMs after the SOC balancing was completed during the

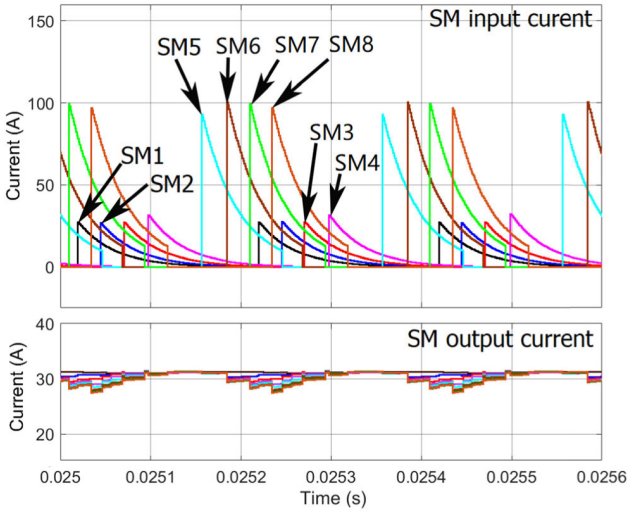

FIGURE 9. Simulation current waveforms of the SMs before SOC balancing was completed during the discharging process.

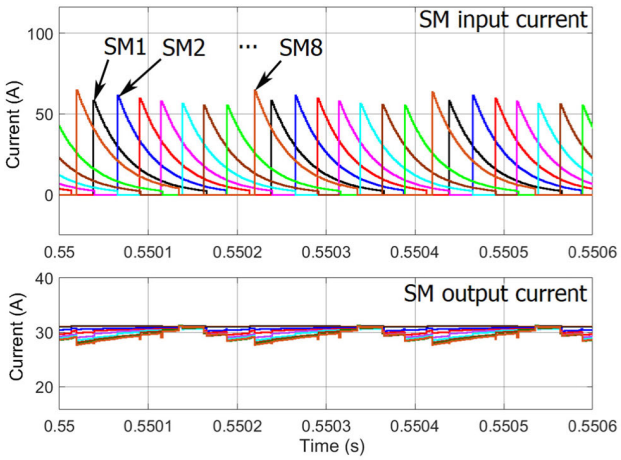

FIGURE 10. Simulation current waveforms of the SMs after SOC balance was completed during the discharging process.

discharging process. At t = 0.55s, the SOC of the battery has been basically balanced. The input currents of the eight SMs are not much different, and the eight stacks are evenly discharged to maintain the SOC balance of the battery.

It can be seen from Figure 9 and Figure 10 that no matter how the input current of the SM changes, its output current can basically remain stable, because the size of the SM output current is determined by the external DC-DC load. Therefore, when the RFB is discharged, if the SOC of one or several stacks is higher than other stacks, increase the discharge current of these stacks, and these stacks will discharge more. When the RFB is charged, if the SOC of one or several stacks is higher than other stacks, reducing the charging time of these stacks will decrease the charging capacity of these stacks. In this way, the energy consumption of the pump is used to balance the SOC of the battery, and no energy is wasted.

Figure 11 presents a part of the simulation waveforms of one SM. They are: currents of MOSFET T_1, T_2, and T_3; Current and voltage of capacitor C; Input and output current of SM; PWM pulse of MOSFET T_1.

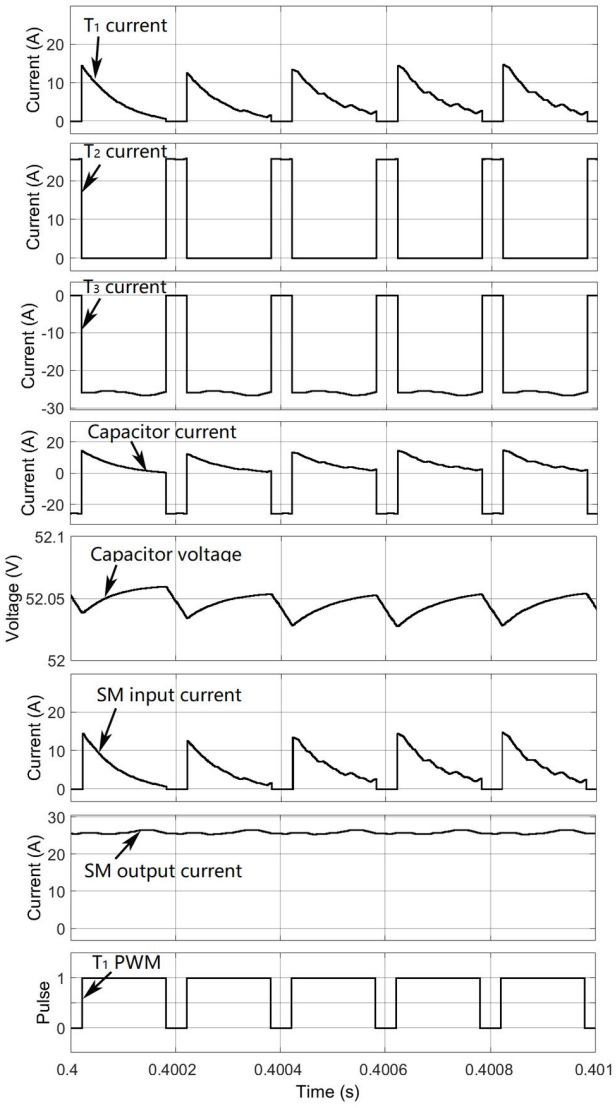

FIGURE 11. Simulation waveforms of one sub-module (part 1).

The balancing circuit alternatively configures the SM in charge-state for absorbing energy from the stacks of battery, and then in discharge-state for releasing energy to DC-DC converter to drive the circulating pump.

For charge-state, the capacitor is connected to the stack of the battery to charge. MOSFET T_1 and T_3 are turned on, and T_2 is turned off. The MOSFET current i_{T1} comes from the battery current i_{BATT}, and is equal to the capacitor current i_C. Therefore, the MOSFET current i_{T1} decreases exponentially and capacitor voltage u_C increases exponentially. The MOSFET current i_{T2} is zero because T_2 is turned off, and the MOSFET current i_{T3} is negative due to freewheeling.

For discharge-state, the capacitor releases energy to the DC-DC converter to drive the circulating pump. MOSFET

T_1 and T_3 are turned off, and T_2 is turned on. The MOSFET current i_{T2} comes from the capacitor current i_C, and is equal to the DC-DC current i_{DC-DC}. Therefore, the capacitor voltage u_C decreases with the discharging time. Meanwhile, the MOSFET current i_{T1} and i_{T3} both are zero because T_1 and T_3 are turned off.

It is easy to see that the input current of the sub-module i_{BATT} is intermittent, but the output current i_{DC-DC} is continuous.

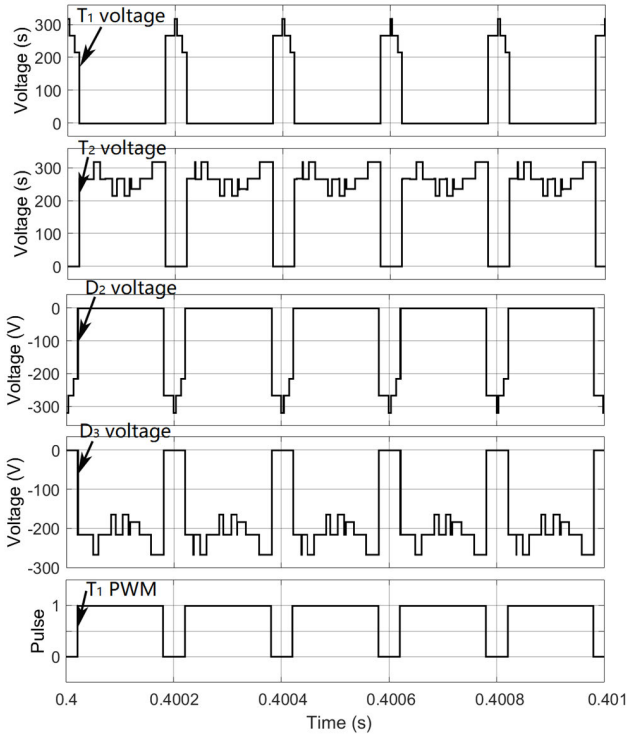

FIGURE 12. Simulation waveforms of one sub-module (part 2).

Figure 12 shows other parts of the simulation waveforms of one SM. They are: voltages of MOSFET T_1 and T_2; Voltage of diode D_2 and D_3; PWM pulse of MOSFET T_1.

It is easy to know that the voltage stress of MOSFETs and diodes change continuously with the switching states of the SMs, and the maximum voltage stress of the MOSFETs and diodes is about 350V, which is consistent with the conclusion of Equation (17).

In a word, the simulation results prove the correctness and effectiveness of the proposed circuit and its control strategy.

V. EXPERIMENTAL VERIFICATION

To further verify the effectiveness of the proposed balancing circuit and its control scheme, a downscaled experimental prototype was established in the laboratory, as shown in Figure 13.

The prototype includes the redox flow battery, DC load, modular balancing circuit, etc. The redox flow battery is composed of 12 stacks in series, and the rated voltage of each stack is only 4.8V because there are only three cells in one stack. Each stack is equipped with two independent

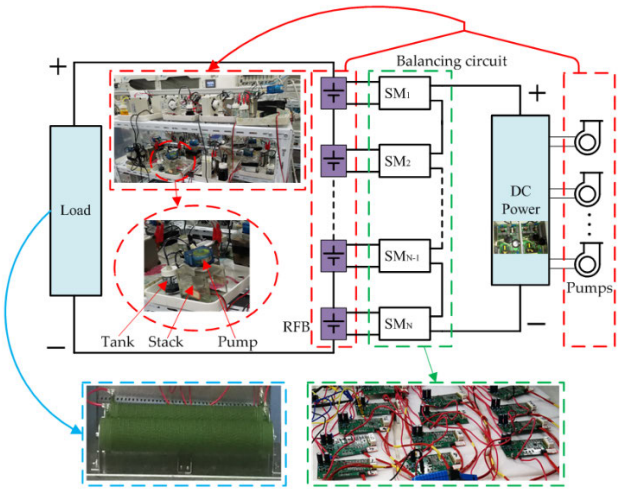

FIGURE 13. The platform of the experimental prototype.

pumps and electrolytes. Detailed parameters of the prototype are listed in Table 5.

TABLE 5. Parameters of simulation model.

Parameter	Value
Rated DC bus voltage (V)	58
Number of stacks	12
Rated voltage of the stack (V)	4.8
Rated capacity of one stack (Ah)	0.5
Number of SMs of balancing circuit	12
Number of cells per stack	3
Rated voltage of one cell (V)	1.6
Control period (μs)	200

It should be noted that the author still has certain difficulties in accurately estimating SOC due to hardware reasons. Thus, this paper temporarily uses the terminal voltage to replace the SOC for battery balance control. In general, the terminal voltage of the RFB decreases as its SOC decreases, and increases as its SOC increases. Therefore, it is acceptable to use terminal voltage instead of SOC to verify the effectiveness of the balancing control strategy.

In order to verify the effectiveness of the balancing control, each stack of the redox flow battery is initially charged to a different voltage, and then discharged. When the redox flow battery discharges, the proposed balancing circuit performs equalizing control immediately.

The experimental results of battery balancing control are shown in Figure 14. In the experiment, the stack voltages of the redox flow battery were collected by sensors and then displayed on the touch screen in curves. And the data was listed in Table 6.

In the beginning, the initial voltage of each stack is different, and its value varies between 4.7V and 5.7V. Then the battery is discharged and balanced, and the voltage value is

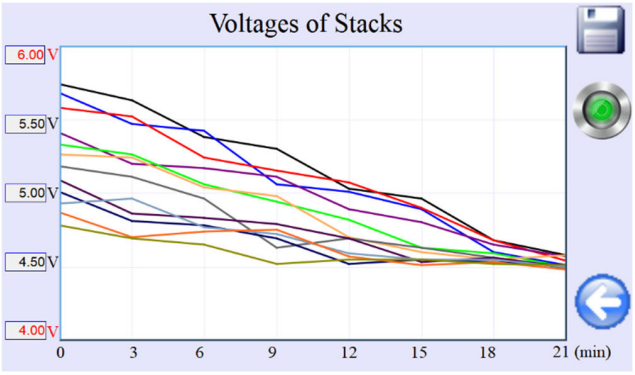

FIGURE 14. Experimental results for the balancing control of redox flow battery.

TABLE 6. Terminal voltage of RFB experimental prototype.

Serial of stack	Initial voltage (V)	Voltage after discharging 9 minutes (V)	Voltage after discharging 18 minutes (V)
SM1	5.74	5.30	4.58
SM2	5.68	5.06	4.51
SM3	5.58	5.15	4.54
SM4	5.41	5.11	4.57
SM5	5.33	4.94	4.50
SM6	5.26	4.98	4.58
SM7	5.18	4.63	4.49
SM8	5.09	4.79	4.50
SM9	5.01	4.69	4.51
SM10	4.93	4.72	4.50
SM11	4.87	4.75	4.48
SM12	4.78	4.65	4.51

sampled and displayed every 3 minutes. It can be seen that the voltages of all stacks tend to be the same after about 21 minutes. Due to the sensor sampling accuracy and the influence of noise interference, the voltage curves are not as smooth as in the simulation model, but in general observation, the purpose of balancing the battery can still be achieved.

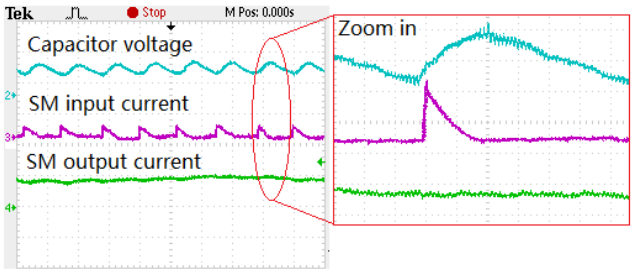

FIGURE 15. Experimental waveforms of the sub-module of the active balancing circuit. CH1: capacitor voltage (5 V/div), CH2: input current of sub-module (5 A/div), CH3: output current (5 A/div). Time scale: 200 ms/div.

Figure 15 shows the experimental waveforms of one sub-module of the balancing circuit. Three channels in the oscilloscope are Channel 1, Channel 2, and Channel 3 from top to bottom. Channel 1 represents the capacitor voltage waveform; Channel 2 shows the input current waveform of the sub-module, which is also the current of MOSFET T_1; Channel 3 gives the output current waveform of the sub-module, which represents the current of MOSFET T_2 when the sub-module is in series with the balancing circuit, or represents the current of MOSFET T_3 when it is bypassed.

It can be seen that the sub-module alternately works in two working states, the charge state and the discharge state. In the charge state, the capacitor is charged through the MOSFET T_1. As the capacitor voltage gradually increases, the charging current gradually decreases. In the discharge state, the capacitor is connected in series in the balancing circuit, and its voltage gradually decreases. At this time, the charging current is zero, indicating that the input-side and the output-side of the sub-module are time-sharing isolated.

It is easy to see that the experimental results verify the effectiveness of the proposed circuit and control strategy.

VI. CONCLUSION

In this paper, a modular active balancing circuit for the redox flow battery is proposed to improve the operation performance and energy conversion efficiency of the redox flow battery applied in the energy storage system. By modular design, the proposed balancing circuit provides a new battery balancing mechanism, which combines the pump driving circuit and the SOC equalization circuit of the redox flow battery, and uses the energy consumed by the pump driving to achieve the SOC balance for the battery. It not only reduces the complexity of the battery control system, but also improves the energy efficiency of the system.

The balancing circuit proposed in this paper has the advantages of high efficiency, high reliability, and good scalability. But it also faces certain challenges. For example: There are many power devices used in this circuit, which will increase the operating cost of the system in the current period. However, the authors believe that the cost of power devices will continue to decrease with the development of semiconductor industry in the future. Therefore, the proposed modular balancing circuit will be very promising in the future.

Simulation and experiment results prove the effectiveness of the proposed balancing circuit and control schemes.

REFERENCES

[1] R. D'Agostino, L. Baumann, A. Damiano, and E. Boggasch, "A vanadium-redox-flow-battery model for evaluation of distributed storage implementation in residential energy systems," *IEEE Trans. Energy Convers.*, vol. 30, no. 2, pp. 421–430, Jan. 2015.

[2] B. K. Samanta, A. Kar, S. Chanda, and A. Bhattacharjee, "Design of DC–DC converter-based interfacing for vanadium redox flow battery," in *Proc. Innov. Energy Manage. Renew. Resour.*, Feb. 2021, pp. 1–6.

[3] B. Xiong, H. Zhang, X. Deng, and J. Tang, "State of charge estimation based on sliding mode observer for vanadium redox flow battery," in *Proc. IEEE Power Energy Soc. Gen. Meeting*, Jul. 2017, pp. 1–5.

[4] M. T. Lawder, B. Suthar, P. W. C. Northrop, S. De, C. M. Hoff, O. Leitermann, M. L. Crow, S. Santhanagopalan, and V. R. Subramanian, "Battery energy storage system (BESS) and battery management system (BMS) for grid-scale applications," *Proc. IEEE*, vol. 102, no. 6, pp. 1014–1030, Jun. 2014.

[5] M. Guarnieri, P. Mattavelli, G. Petrone, and G. Spagnuolo, "Vanadium redox flow batteries: Potentials and challenges of an emerging storage technology," *IEEE Ind. Electron. Mag.*, vol. 10, no. 4, pp. 20–31, Dec. 2016.
[6] B. Xiong, Z. Wang, Y. Li, K. Qin, J. Chen, and J. Mu, "An optimal operational strategy for vanadium redox flow battery based on particle swarm optimization," in *Proc. IEEE Innov. Smart Grid Technol.-Asia (ISGT Asia)*, May 2019, pp. 2639–2643.
[7] A. Clemente, M. Montiel, F. Barreras, A. Lozano, and R. Costa-Castelló, "Vanadium redox flow battery state of charge estimation using a concentration model and a sliding mode observer," *IEEE Access*, vol. 9, pp. 72368–72376, May 2021.
[8] B. Xiong, Y. Yang, J. Tang, Y. Li, Z. Wei, Y. Su, and Q. Zhang, "An enhanced equivalent circuit model of vanadium redox flow battery energy storage systems considering thermal effects," *IEEE Access*, vol. 7, pp. 162297–162308, Nov. 2019.
[9] Z. Wang, B. Xiong, J. Tang, Y. Li, Y. Huang, G. Zhang, and J. Chen, "Multi-parameter optimization strategy for vanadium redox flow battery operation based on genetic algorithm," in *Proc. IEEE 10th Int. Symp. Power Electron. Distrib. Gener. Syst. (PEDG)*, Jun. 2019, pp. 717–721.
[10] M. P. Akter, J. Bao, M. Skyllas-Kazacos, K. S. Alam, D. Xiao, and M. F. Rahman, "Capacitor-less bidirectional synchronous buck-boost converter for vanadium redox flow battery," in *Proc. 29th Australas. Universities Power Eng. Conf. (AUPEC)*, Nov. 2019, pp. 1–6.
[11] B. R. Chalamala, T. Soundappan, G. R. Fisher, M. R. Anstey, V. V. Viswanathan, and M. L. Perry, "Redox flow batteries: An engineering perspective," *Proc. IEEE*, vol. 102, no. 6, pp. 976–999, Jun. 2014.
[12] B. Xiong, J. Zhao, Y. Su, Z. Wei, and M. Skyllas-Kazacos, "State of charge estimation of vanadium redox flow battery based on sliding mode observer and dynamic model including capacity fading factor," *IEEE Trans. Sustain. Energy*, vol. 8, no. 4, pp. 1658–1667, Oct. 2017.
[13] A. Trovo, V. Di Noto, J. E. Mengou, C. Gamabaro, and M. Guarnieri, "Fast response of kW-class vanadium redox flow batteries," *IEEE Trans. Sustain. Energy*, early access, Jul. 14, 2021, doi: 10.1109/TSTE.2021.3096573.
[14] M. Bahloul, A. Majumdar, and S. K. Khadem, "An improved SoC controller for flow battery based ESS to provide efficient grid services," in *Proc. 1st Global Power, Energy Commun. Conf. (GPECOM)*, Jun. 2019, pp. 380–385.
[15] Y. R. Challapuram, G. M. Quintero, S. B. Bayne, A. S. Subburaj, and M. A. Harral, "Electrical equivalent model of vanadium redox flow battery," in *Proc. IEEE Green Technol. Conf. (GreenTech)*, Apr. 2019, pp. 1–4.
[16] X. Li, Y. Mo, N. Di, and Y. Oiu, "Equalization charge-discharge control strategy for series-connected vanadium redox flow batteries based on LC oscillation circuit," in *Proc. IEEE 3rd Adv. Inf. Technol., Electron. Automat. Control Conf. (IAEAC)*, Oct. 2018, pp. 2018–2022.
[17] D. Han, K. Yoo, P. Lee, S. Kim, S. Kim, and J. Kim, "Equivalent circuit model considering self-discharge for SoC estimation of vanadium redox flow battery," in *Proc. 21st Int. Conf. Electr. Mach. Syst. (ICEMS)*, Oct. 2018, pp. 2171–2176.
[18] X. Qiu, T. A. Nguyen, J. D. Guggenberger, M. L. Crow, and A. C. Elmore, "A field validated model of a vanadium redox flow battery for microgrids," *IEEE Trans. Smart Grids*, vol. 5, no. 4, pp. 1592–1601, Jul. 2014.
[19] L. Li, C. Sun, and J. Wu, "Charge capacity management in redox flow battery string," U.S. Patent 2016 0 006 052, Jan. 7, 2016.
[20] S. Y. Reece, P. Badrinarayanan, N. Tyagi, and T. B. Grejtak, "Electrolyte balancing strategies for flow batteries," U.S. Patent 2019 0 207 236, Jul. 4, 2019.
[21] K. Wei and L. Li, "Redox flow battery systems including a balance arrangement and methods of manufacture and operation," U.S. Patent 2020 0 373 602, Nov. 26, 2020.
[22] Y. Shang, S. Zhao, Y. Fu, B. Han, P. Hu, and C. C. Mi, "A lithium-ion battery balancing circuit based on synchronous rectification," *IEEE Trans. Power Electron.*, vol. 35, no. 2, pp. 1637–1648, Feb. 2020.
[23] M. Liu, Y. Chen, Y. Elasser, and M. Chen, "Dual frequency hierarchical modular multilayer battery balancer architecture," *IEEE Trans. Power Electron.*, vol. 36, no. 3, pp. 3099–3110, Mar. 2021.
[24] S. Narayanaswamy, M. Kauer, S. Steinhorst, M. Lukasiewycz, and S. Chakraborty, "Modular active charge balancing for scalable battery packs," *IEEE Trans. Very Large Scale Integr. (VLSI) Syst.*, vol. 25, no. 3, pp. 974–987, Mar. 2017.
[25] A. Trovo and M. Guarnieri, "Battery management system with testing protocols for kW-class vanadium redox flow batteries," in *Proc. 2nd IEEE Int. Conf. Ind. Electron. Sustain. Energy Syst. (IESES)*, Sep. 2020, pp. 33–38.
[26] G. Dong, F. Yang, K.-L. Tsui, and C. Zou, "Active balancing of lithium-ion batteries using graph theory and A-star search algorithm," *IEEE Trans. Ind. Informat.*, vol. 17, no. 4, pp. 2587–2599, Apr. 2021.
[27] T. Zheng, S. Gui, X. Li, T. Sheng, and D. Wei, "SoC equalization control scheme of all vanadium redox flow battery," (in Chinese), *Chin. J. Power Sources*, vol. 42, no. 1, pp. 81–83, Jan. 2018.
[28] X. Li, N. Wang, X. Chen, and D. Wei, "Balanced control strategy and simulation of large capacity all vanadium redox flow battery," (in Chinese), *Power Electron.*, vol. 50, no. 11, pp. 53–56, Nov. 2016.
[29] H. Zhao, H. Zhang, X. Ma, J. Shao, H. Wang, and T. Chigan, "Flow battery system and large scale flow battery energy storage device," U.S. Patent 2019 0 288 320, Sep. 19, 2019.
[30] U. Richard, W. Adam, and R. Peter, "Flow battery and a method for balancing the SoC," WO Patent 2020 030 762, Feb. 13, 2020.
[31] B. Xu, L. Zhang, and W. Ji, "Improved non-singular fast terminal sliding mode control with disturbance observer for PMSM drives," *IEEE Trans. Transport. Electrific.*, early access, May 26, 2021, doi: 10.1109/TTE.2021.3083925.
[32] Q. Hou and S. Ding, "GPIO based super-twisting sliding mode control for PMSM," *IEEE Trans. Circuits Syst. II, Exp. Briefs*, vol. 68, no. 2, pp. 747–751, Feb. 2021.
[33] N. Ullah, Z. Farooq, I. Sami, M. S. Chowdhury, K. Techato, and H. I. Alkhammash, "Industrial grade adaptive control scheme for a microgrid integrated dual active bridge driven battery storage system," *IEEE Access*, vol. 8, pp. 210435–210451, Nov. 2020.
[34] D. Arcos-Aviles, J. Pascual, F. Guinjoan, L. Marroyo, G. García-Gutiérrez, R. Gordillo-Orquera, J. Llanos-Proaño, P. Sanchis, and T. E. Motoasca, "An energy management system design using fuzzy logic control: Smoothing the grid power profile of a residential electro-thermal microgrid," *IEEE Access*, vol. 9, pp. 25172–25188, 2021.
[35] M. Zhao, R. Zhang, C. Lin, H. Zhou, and J. Shi, "Stochastic model predictive control for dual-motor battery electric bus based on signed Markov chain Monte Carlo method," *IEEE Access*, vol. 8, pp. 120785–120797, Jul. 2020.

WEIDE GUAN was born in Jiangsu, China. He received the M.S. degree in mechanical engineering from Southeast University, Nanjing, China, in 2009, and the Ph.D. degree in electrical engineering from Hunan University, Changsha, China, in 2019. From July 2009 to August 2015, he was a Senior Engineer with Wasion Group, Changsha. From March 2016 to March 2017, he was a Visiting Scholar with The Ohio State University, Columbus, OH, USA. He is currently a Lecturer of electrical engineering with the School of Electrical and Information Engineering, Changsha University of Science and Technology. His research interests include applications of power electronics, electric vehicle control, and wind power generation technology.

XIAOQING HUANG was born in Hunan, China, in 1981. She received the Ph.D. degree in electrical engineering from Southeast University, Nanjing, China, in 2009. She is currently an Associate Professor of electrical engineering with the College of Electrical and Information Engineering, Hunan University. Her current research interests include the power systems, wind power generation technology, and the ac/dc energy conversion technology.